ISSN 1674-1056
http://cpb.iphy.ac.cn
http://iopscience.iop.org/cpb
中国物理 B
Chinese Physics
中国物理 Chinese Physics B

Flexible rGO/Fe_3O_4 NPs/polyurethane film with excellent electromagnetic properties

Wei-Qi Yu(余维琪), Yi-Chen Qiu(邱怡宸), Hong-Jun Xiao(肖红君), Hai-Tao Yang(杨海涛), Ge-Ming Wang(王戈明)
Citation: Chin. Phys. B . 2019, 28(10): 108103 . **doi:** 10.1088/1674-1056/ab4041
Journal homepage: http://cpb.iphy.ac.cn; http://iopscience.iop.org/cpb

What follows is a list of articles you may be interested in

Free-standing, curled and partially reduced graphene oxide network as sulfur host for high-performance lithium-sulfur batteries

Hui-Liang Chen(陈辉亮), Zhuo-Jian Xiao(肖卓建), Nan Zhang(张楠), Shi-Qi Xiao(肖仕奇), Xiao-Gang Xia(夏晓刚), Wei Xi(席薇), Yan-Chun Wang(王艳春), Wei-Ya Zhou(周维亚), Si-Shen Xie(解思深)
Chin. Phys. B . 2018, 27(6): 068101 . **doi:** 10.1088/1674-1056/27/6/068101

Metal-enhanced fluorescence of graphene oxide by palladium nanoparticles in the blue-green part of the spectrum

A Omidvar, M R RashidianVaziri, B Jaleh, N Partovi Shabestari, M Noroozi
Chin. Phys. B . 2016, 25(11): 118102 . **doi:** 10.1088/1674-1056/25/11/118102

Synthesis of graphene-supported monodisperse AuPd bimetallic nanoparticles for electrochemical oxidation of methanol

Xiao Hong-Jun, Shen Cheng-Min, Shi Xue-Zhao, Yang Su-Dong, Tian Yuan, Lin Shao-Xiong, Gao Hong-Jun
Chin. Phys. B . 2015, 24(7): 078109 . **doi:** 10.1088/1674-1056/24/7/078109

Liquid-phase and solid-phase microwave irradiations for reduction of graphite oxide

Zhao Na, Wen Chen-Yu, Zhang David Wei, Wu Dong-Ping, Zhang Zhi-Bin, Zhang Shi-Li
Chin. Phys. B . 2014, 23(12): 128101 . **doi:** 10.1088/1674-1056/23/12/128101

Complete coverage of reduced graphene oxide on silicon dioxide substrates

Huang Jingfeng, Melanie Larisika, Chen Hu, Steve Faulkner, Myra A. Nimmo, Christoph Nowak, Alfred Tok Iing Yoong
Chin. Phys. B . 2014, 23(8): 088104 . **doi:** 10.1088/1674-1056/23/8/088104

Flexible rGO/Fe_3O_4 NPs/polyurethane film with excellent electromagnetic properties*

Wei-Qi Yu(余维琪)[1,2], Yi-Chen Qiu(邱怡宸)[3], Hong-Jun Xiao(肖红君)[2,†], Hai-Tao Yang(杨海涛)[3,4], and Ge-Ming Wang(王戈明)[1,‡]

[1] School of Materials Science and Engineering, Wuhan Institute of Technology, Wuhan 430205, China
[2] National Center for Nanoscience and Technology, Beijing 100190, China
[3] Beijing National Laboratory for Condensed Matter Physics, Institute of Physics, Chinese Academy of Sciences, Beijing 100190, China
[4] Fujian Institute of Innovation, Chinese Academy of Sciences, Fozhou 350108, China

(Received 21 July 2019; revised manuscript received 24 August 2019; published online 25 September 2019)

Large-area and flexible reduced graphene oxide (rGO)/Fe_3O_4 NPs/polyurethane (PU) composite films are fabricated by a facile solution-processable method. The monolayer assembly of Fe_3O_4 nanoparticles with a high particle-stacking density on the graphene oxide (GO) sheets is achieved by mixing two immiscible solutions of Fe_3O_4 nanoparticles in hexane and GO in dimethylformide (DMF) by a mild sonication. The x-ray diffraction and Raman spectrum confirm the reduced process of rGO by a simple thermal treatment. The permittivity value of the composite in a frequency range of 0.1 GHz–18 GHz increases with annealing temperature of GO increasing. For 5-wt% rGO/Fe_3O_4 NPs/PU, the maximum refection loss (RL) of over −35 dB appears at 4.5 GHz when the thickness of film increases to 5 mm. The rGO/Fe_3O_4 NPs/PU film, exhibiting good electromagnetic properties over GHz frequency range, could be a potential candidate as one of microwave absorption materials in flexible electronic devices.

Keywords: graphene oxide, magnetic nanoparticles, flexible film, electromagnetic properties

PACS: 81.05.ue, 75.75.–c, 67.80.dm, 92.60.Ta **DOI:** 10.1088/1674-1056/ab4041

1. Introduction

In recent years, with the rapid development of the modern communication technologies, especially 5G wireless communication, electronic components such as miniature filters, integrated inductor, microchip antenna, and electromagnetic interference (EMI) devices have been required to have the characteristics such as miniaturization, high-speed, low energy-consumption, good electromagnetic wave absorption, and flexibility.[1–5] There is a growing demand for the magnetic materials with high resonance frequency (f_r), large permeability (μ), and suitable magnetic loss in a GHz frequency range to be used as inductor cores, antenna substrates, and a wide range of other microwave devices in size reduction and minimizing the electromagnetic energy trapped in the devices.[6] For example, magnetic materials can be used to reduce the volume of microchip antennas because it is roughly inversely proportional to the refractive index $n = (\varepsilon'\mu')^{1/2}$, in which ε' and μ' are the real part of permittivity and permeability, respectively.[7,8] To fabricate the electromagnetic (EM) absorption material with large EM absorption ratio, the material should have a strong absorption capability and good impedance matching of permittivity and permeability. The high electronic resistivity of magnetic nanomaterials dispersed into a polymeric matrix will also reduce the eddy current loss significantly, and potentially increase the quality factor (Q factor) of a fabricated component. This opens the way for fabricating the miniaturized and flexible integrated antennas and inductors at high frequencies.[9]

In addition, carbon nanotube (CNT)- and graphene-based composites have become new candidates for electromagnetic functional materials including microwave absorbing materials.[10,11] Generally, the enhanced microwave absorption of these materials can be mainly attributed to the following aspects: the residual defects on the surface of the graphene oxide (GO) sheets, the large aspect ratio and high conductivity, interfacial polarizations in these composites. Good EM absorption properties of reduced graphene oxide (rGO) or its related materials have been demonstrated. Zhang *et al.* have reported that an ultralight and highly compressible graphene foam has a broadband and tunable high-performance microwave absorption property.[12] Chen *et al.* have reported that novel reduced GO (RGO) composites with hematite nanoparticles embedded in RGO layers and wrapped by RGO sheets exhibited remarkably improved electromagnetic absorbing performance.[13] Many other composites, such as rGO/α-Fe_2O_3,[14] PVDF/GO,[15] and rGO/ZnO hollow spheres[16] have been reported as EM absorption materials.

*Project supported by the National Natural Science Foundation of China (Grant Nos. 11274370, 51471185, and 11704288) and the National Key Research and Development Program of China (Grant Nos. 2016YFJC020013 and 2018FYA0305800).

†Corresponding author. E-mail: xiaohj@nanoctr.cn
‡Corresponding author. E-mail: wanggemingwit@163.com

© 2019 Chinese Physical Society and IOP Publishing Ltd

Though they usually have good EM absorption properties, poor dispersity and stability, and large loading content of GO or rGO, are the severe drawbacks to impede their practical applications. In addition, most of researchers use paraffin as matrix to measure the EM absorption, which cannot provide the practical EM parameters in the electronic devices to demonstrate their real EM absorption properties.

Here in this work, we prepare monodisperse Fe_3O_4 nanoparticles (NPs) and fabricate large-area rGO/Fe_3O_4 NPs/PU flexible film by using a facile solution-processable method. Fe_3O_4 NPs has recently attracted much attention due to its high Curie temperature ($T_c \sim 850$ K), high magnetic moment, and relatively good air-stability.[17–20] PU is widely used in electronic area due to its good mechanical properties, anti-aging properties, and suitable dielectronic properties.[21,22] GO and PU can sufficiently disperse in dimethylformamide and form the strong interfacial bonding among rGO, Fe_3O_4 NPs, and PU. The flexible composited film shows excellent microwave absorption properties due to the interfacial polarization, charge transfer effect, and good impedance matching.

2. Experiment

2.1. Materials

FeO·OH (50 mesh–80 mesh), 1-octadencene (ODC), oleic acid (OA), graphite powder (150 mesh) were purchased from Aldrich-sigma Chemical Co. $KMnO_4$, $K_2S_2O_8$, P_2O_5, H_2O_2 were purchased from Sinopharm Chemical ReagentCo., Ltd, polyurethane was purchased from Sinopec Shanghai petrochemical Co., Ltd. All chemicals were analytical grade and used directly without further purification.

2.2. Preparation of Fe_3O_4 NPs

The monodispersive Fe_3O_4 NPs were synthesized on a gram scale according to our reported method.[23] In a typical experiment for 7-nm NPs, 0.528 g (6 mmol) of FeO·OH, 10.296-g OA (36 mmol), and 40 mL of ODC were combined in the three-neck round-bottom reaction flask. The mixture was heated to 315 °C with a heating rate of 10 °C/min under magnetically stirring, and refluxed at the temperature for 1 h. The reaction solution was then cooled to room temperature by removing the heat source. Under air condition, ethanol and acetone were added to the mixture, and a black material was separated via centrifugation. Centrifugation (3000 rpm/min) was used to remove any aggregation residue. The product was then precipitated with ethanol, centrifuged (8000 rpm/min) to remove the solvent, excess surfactants and NPs with smaller size, and re-dispersed in hexane.

2.3. Preparation of rGO/Fe_3O_4 NPs and rGO/Fe_3O_4 NPs PU film

GO was synthesized from natural graphite powder by a modified Hummers method.[24,25] Exfoliation was carried out by ultrasonicating the GO dispersion under ambient condition. The as-prepared GO was dispersed in DMF solution. The general procedure to assemble Fe_3O_4 NPs on GO sheets is adopted as follows: 15-mg Fe_3O_4 NPs were dispersed in 20-mL hexane and added into 20-mL DMF solution containing GO (0.5 mg/mL), and then the resulting mixture was dramatically stirred for 5 min and sonicated for another 1 h. After adding 10-mL ethanol, the suspension was centrifuged at 9500 rpm for 10 min to separate the GO/Fe_3O_4 NPs from mixed solvents. The GO/Fe_3O_4 NPs product was annealed at different temperature under Ar flow to obtain rGO/Fe_3O_4 NPs. For the preparation of rGO/Fe_3O_4 NPs/PU film, PU (5 g) was dissolved in DMF (25 mL) at 50 °C under a dramatic mechanical stirring. In another baker, 25 mL of a 10-mg/mL rGO/Fe_3O_4 NPs suspension in DMF was ultrasonicated for 30 min. Then, the black rGO/Fe_3O_4 NPs suspension was slowly added into the PU solution and sonicated for another 30 min. Then, the homogeneous rGO/Fe_3O_4 NPs/PU solution was scraped into a smooth film by adjusting its viscosity. The film was dried in vacuum drying box at 60 °C until no weight lost.

3. Characterization

The x-ray diffraction (XRD) data were collected on a D2 PHASER x-ray diffractometer (Cu Kα radiation, $\lambda = 0.154$ nm) at 40 kV and 30 mA. The morphology of the sample was investigated by transmission electron microscopy (TEM, JEM-2100F with operation voltage 200 kV). Raman spectra were obtained with a Renishaw Raman system model in Via-Reflex spectrometer and a LabRam HR 800 spectrometer of HORIBA Co. The 532-nm radiation from a solid-state laser was used as an excitation source. For magnetic and dielectric spectrum measurements, the rGO/Fe_3O_4 NPs/PU film was processed into an annulus film with an outer diameter $\phi_{outer} = 7.00$ mm and an inner diameter $\phi_{inner} = 3.04$ mm. The scattering parameters (S_{11} and S_{21}) were measured by a vector network analyzer (Agilent N5224A) through using a coaxial transmission–reflection method in a frequency range of 0.1 GHz–18 GHz. The complex permeability (μ_r) and permittivity (ε_r) were determined from the scattering parameters by using the Nicolson models.

4. Results and discussion

Figure 1(a) shows the typical TEM images of few-layered GO prepared by a mild sonic exfoliation with the oxidization in advance to increase the interspace of graphite. The bright

spots shown in the selected area electron diffraction (SAED) pattern indicate that the GO has a good crystalline structure after being exfoliated. The Fe_3O_4 NPs prepared by the high-temperature organic solution method have a narrow size distribution with an average diameter of 7.0 ± 0.5 nm as shown in Fig. 1(b). Such monodisperse Fe_3O_4 NPs with uniform size and shape can have uniform electromagnetic response. In Fig. 1(c), we can observe that the Fe_3O_4 NPs directly form monolayer assembly on the surface of GO sheets with a low cover density, when Fe_3O_4 NPs with a low concentration of 0.75 mg/mL in hexane were mixed with the DMF dispersion of GO sheets under a mild sonication. It should be noted that the multiply-layer assembly phenomena of Fe_3O_4 NPs on GO sheets can be observed by mixing the chloroform solution of Fe_3O_4 NPs and the DMF dispersion of GO sheets. It appeared that mixing two immiscible solutions in hexane and DMF via sonication was an essential step to realize monolayer assemble of Fe_3O_4 NPs on GO sheets.[26] If the concentration of Fe_3O_4 NPs in hexane increases to 1.5 mg/mL, the monolayer assembly of Fe_3O_4 NPs with a high stacking density can be observed, which demonstrates that this method can realize the high-density loading on the GO sheets.

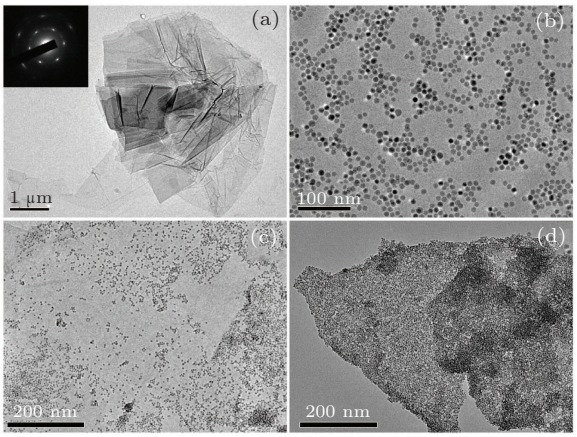


Fig. 1. TEM images of (a) GO sheet, with inset showing SAED pattern; (b) monodisperse Fe_3O_4 NPs; (c) low- and (d) high-stacking-density monolayer assembly of Fe_3O_4 NPs on GO nanosheet.

To improve the interface binding strength and permittivity properties, GO/Fe_3O_4 NPs are annealed at moderate temperatures to form rGO/ Fe_3O_4 NPs. If being annealed at above 600 °C, Fe_3O_4 NPs will aggregate and result in a wide size distribution. As shown in Figs. 2(a) and 2(b), the GO/Fe_3O_4 NPs are annealed at 300 °C and 500 °C, respectively. After being annealed at 300 °C, the Fe_3O_4 NPs keep their size unchanged, but undergo a slight change in shape: from the sphere to polygon. Since the shape observed in TEM is a project two-dimensional (2D) image, the Fe_3O_4 NPs should change their shape from truncated icosahedron to polyhedron after being annealed at 300 °C. After being annealed at 500 °C, the Fe_3O_4 NPs shows their size obviously increases to 9.0 ± 0.5 nm with some big NPs and their shape also becomes polyhedron. Figure 2(c) shows, the XRD patterns of the as-prepared and annealed GO, together with the pristine graphite. The (002) peak intensity of graphite is much large and the other peaks cannot well be shown if the whole (002) peak is included in Fig. 2(c). The diffraction peak around 26.48 for graphite disappears in the pattern of GO and a broad peak is present at $2\theta = 10.98$, indicating the successful oxidation of raw graphite into graphite oxide.[25,27,28] After annealing, the diffraction peaks at $2\theta = 10.98$ disappears and a broad peak forms and moves closer to $2\theta = 26.48$ after 500 °C annealing than after 300 °C annealing. This indicates that the GO nanosheets can be reduced to rGO only by the simple high-temperature annealing. Figure 2(d) shows the Raman spectrum of the GO and rGO/Fe_3O_4 composites. There are two characteristic peaks located at around 1350 cm^{-1} and 1597 cm^{-1} which are attributed to the D and G band of GO. Comparing with pure GO, two weak peaks appear at 281 cm^{-1} and 678 cm^{-1} for the rGO/Fe_3O_4, which is due to the existence of Fe_3O_4. The intensity ratio of the D band to the G band for GO and rGO/Fe_3O_4 annealed at 300 °C and 500 °C are 0.92, 0.86, and 0.81, respectively, indicating that the annealing treatment can remote some oxygen-containing groups and reduce the disordered stacking of GO sheets.[29] Meanwhile, the location of D and G band are observed to shift to the lower wavenumbers, recovering the hexagonal structures of carbon atoms. It should also be noted that the saturation magnetization (M_s) of rGO/Fe_3O_4 NPs can be increased from 55 emu/g of the as-prepared sample to 72 emu/g of 500 °C annealed sample. The rGO/Fe_3O_4 NPs with higher M_s can achieve larger μ' since $\mu' - 1 = M_s^2/2K_u$ showing that μ' increases with M_s increasing. In the expression, K_u is the magnetic anisotropy.

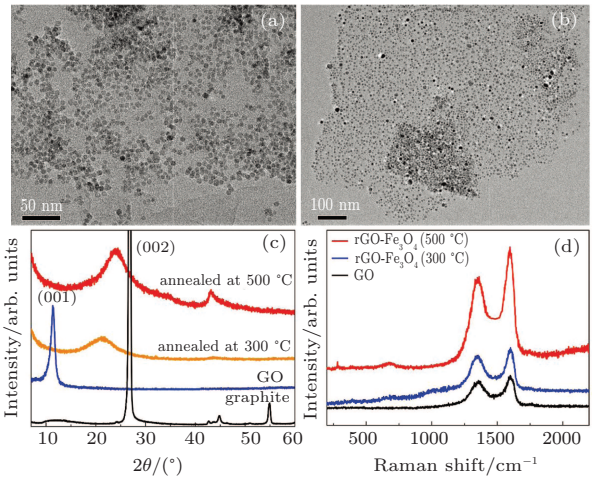


Fig. 2. TEM images of rGO/Fe_3O_4 NPs annealed at (a) 300 °C and (b) 500 °C. (c) The XRD patterns of pristine graphite, as-prepared GO, GO annealed at 300 °C and 500 °C. (d) Raman spectra of GO, rGO/Fe_3O_4 NPs annealed at 300 °C and 500 °C.

Figure 3(a) shows the picture of the smooth thin PU film with a thickness of 0.5 mm and a length of 15 cm contain-

ing 5-wt% rGO/Fe_3O_4 NPs annealed at 300 °C. The thickness of the film can well be controlled in a range from 0.1 mm to 2 mm by adjusting the height of the scraper in our home-made linear glue spreading machine controlled with a precise stepping motor as shown in Fig. 3(b). The film has good flexible properties with a bending angle of 180° as shown in Fig. 3(c). Moreover, the film can be cut into different shapes, which is greatly convenient for the practical application.

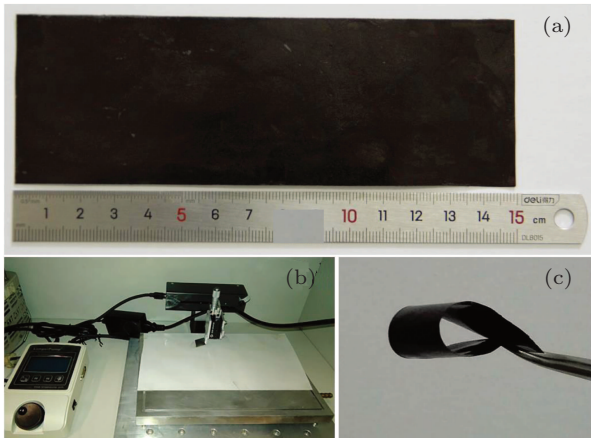


Fig. 3. Pictures of (a) 15-cm-long rGO/Fe_3O_4 NPs/PU film, (b) our home-made scraping film facility, and (c) freely folding rGO/Fe_3O_4 NPs/PU film.

Figures 4(a) and 4(b) show the frequency dependence of the permittivity and permeability for the pure PU film and PU film containing 5 wt% rGO/Fe_3O_4 NPs annealed at 300 °C and 500 °C (named as rGO/Fe_3O_4 NPs/PU-300 and rGO/Fe_3O_4 NPs/PU-500). Figure 4(a) shows that the real part (ε') of relative complex permittivity ($\varepsilon_r = \varepsilon' - j\varepsilon''$) for the pure PU film, rGO/Fe_3O_4 NPs/PU-300, and rGO/Fe_3O_4 NPs/PU-500 decrease from 4.3 to 3.0, 8.2 to 3.9, and 26.1 to 5.9, with the increasing frequency in the range of 0.1 GHz–18 GHz, respectively. The value of ε' significantly increases with the rise of annealing temperature of GO in the composites because the higher temperature leads the quantity of GO to decrease more greatly, which results in the increase of the dipolar polarization and electrical conductivity. The value of the imaginary part (ε'') corresponding to pure PU, rGO/Fe_3O_4 NPs/PU-300, and rGO/Fe_3O_4 NPs/PU-500 are in a range of 0.02–0.33, 1.69–0.73, and 19.26–2.14, respectively. The larger value of ε'' means that the better EM wave absorption property. From Fig. 4(b), it can be seen that the value of μ' of PU is nearly a constant in the whole frequency range from 0.1 GHz to 18 GHz. The value of μ'' of rGO/Fe_3O_4 NPs/PU-500 is larger than that of rGO/Fe_3O_4 NPs/PU-300 below 0.5 GHz. While the rGO/Fe_3O_4 NPs/PU-300 shows that the value of μ' decreases slower with frequency increasing to above 0.5 GHz and the cut-off frequency of about 5 GHz is higher than 3 GHz of rGO/Fe_3O_4 NPs/PU-500 whose value of μ' decreases fast due to the large Fe_3O_4 particles sizes of rGO/Fe_3O_4 NPs/PU-500. According to our previous research,[30] Fe_3O_4 NPs with large sizes have low blocking resonance frequency due to the superparamagnetic behavior. It should be noted that the value of μ' of rGO/Fe_3O_4 NPs/PU film is 5 wt% larger than that of pure Fe_3O_4 NPs dispersed in the PU with the same mass ratio since the higher stacking density on the GO can achieve the strong dipolar–dipolar magnetic interaction.

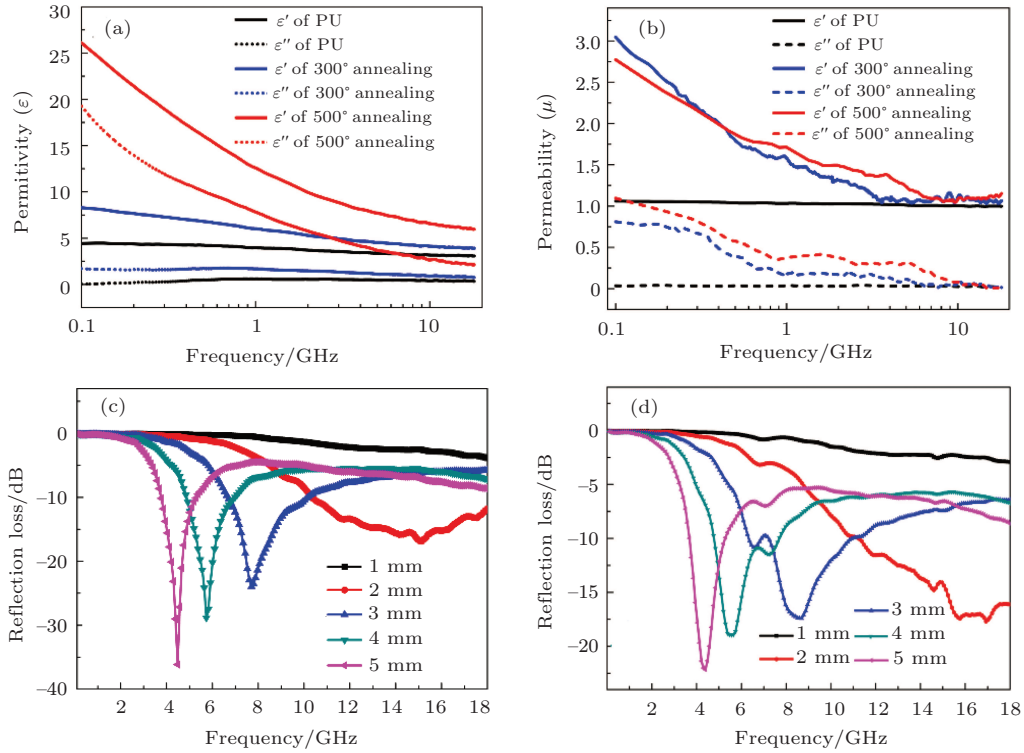


Fig. 4. (a) Frequency-dependent relative complex permittivity and (b) frequency-dependent relative complex permeability. Frequency-dependent RL for the rGO/Fe_3O_4 NPs/PU films with different thicknesses, annealed at 300 °C (c) and at 500 °C (d).

Table 1. Comparison of EM absorption properties of rGO/Fe_3O_4 NPs/PU film with other reported results.

Materials	Max. ε'	Max. ε''	Max. μ'	Max. μ''	Maximum RL/dB	Ref.
rGO/Fe_2O_3	11 at 2 GHz	3.5 at 2 GHz–16 GHz	1	near to 0	−38 dB at 14.8 GHz/2 mm; −25 dB at 4.5 GHz/5 mm with 70% weight ratio	[14]
N-doped GC	11.7 at 2 GHz	3.7 at 2 GHz–16 GHz	1	near to 0	−25 dB at 14.2 GHz/2 mm; −32 dB at 6.0 GHz/4 mm with 10% weight ratio	[10]
Hollow Fe@C	6 at 2 GHz	5.5 at 2 GHz–16 GHz	1.1	0.18	−54.4 dB at 8.8 GHz/4.5 mm; with 30% weight ratio	[29]
N-rGA/Ni	16 at 2 GHz	5 at 2 GHz–16 GHz	1	Less than 0	−30 dB at 12.0 GHz/2 mm; −20 dB at 4.0 GHz/5 mm with 10% weight ratio	[30]
rGO/Fe_3O_4 NPs/PU film	12.5 at 2 GHz	6.0–2.1 at 2 GHz–18 GHz	1.5 at 2 GHz	0.3	−17.5 dB at 16 GHz/2 mm; −35 dB at 4.5 GHz/5 mm with 5% weight ratio	this work

According to the transmission line theory, for a single layer absorber with a backed metal plate, the refection loss (RL) curves are simulated from the electromagnetic parameters at various sample thickness values by means of the following expressions[31,32]

$$Z_{\text{in}} = \sqrt{\frac{\mu_{\text{r}}}{\varepsilon_{\text{r}}}} \tanh\left[\text{j}\left(\frac{2\pi f d}{c}\right)\sqrt{\mu_{\text{r}}\varepsilon_{\text{r}}}\right], \tag{1}$$

$$RL = 20\log\left|\frac{Z_{\text{in}}-1}{Z_{\text{in}}+1}\right|, \tag{2}$$

where f is the frequency of the electromagnetic wave, d is the thickness of sample, c is the velocity of light in free space, Z is the impedance of air, and Z_{in} is the input impedance of the sample. Figures 4(c) and 4(d) show the calculated theoretical RLs of rGO/Fe_3O_4 NPs/PU-300 and rGO/Fe_3O_4 NPs/PU-500 films with different thicknesses in a range of 0.1 GHz–18 GHz. With the thickness increasing, the maximum RL shows an obvious improvement and shifts towards a lower frequency since the absorption meets the phase match conditions based on the quarter-wavelength or three-quarter attenuation.[33] The rGO/Fe_3O_4 NPs/PU-500 film has a better absorption property when the thickness is smaller than 2 mm. While the thickness is larger than 2 mm, the rGO/Fe_3O_4 NPs/PU-300 film has larger RL values and concentrated absorption ranges than those of rGO/Fe_3O_4 NPs/PU-500 film, specifically, over 35 dB at a thickness of 5 mm. It can be attributed to the good impedance match in the rGO/Fe_3O_4 NPs/PU-300 film in the GHz range.[34] The multiple absorption peaks in the rGO/Fe_3O_4 NPs/PU-500 film appear due to the wide size distribution of Fe_3O_4 NPs and strong dielectronic loss. When the thickness of film is 2 mm, the bandwidths of RL value below −10 dB (90% of EM wave absorption) can exceed 6.0 GHz. In addition, for EM wave absorbing composites, dielectric material such as PU and PVA with good wave-transparent properties can guarantee the broadband for EM wave absorbing. The electromagnetic properties of rGO/Fe_3O_4 NPs/PU flexible film are compared with the recently reported results[35,36] as indicated in Table 1. From this table, we can find that rGO/Fe_3O_4 NPs/PU only with 5% weight ratio can have comprehensive EM wave absorption properties, which means achieving light absorbing materials. Thus, the rGO/Fe_3O_4 NPs/PU flexible film with small loading ratio exhibits the excellent EM wave absorption properties due to the synergistic effect of three components of rGO, Fe_3O_4 NPs and PU.

5. Conclusions

In this work, monodisperse magnetic Fe_3O_4 NPs are prepared by a facile high-temperature organic solution method and loaded on the GO with a high monolayer stacking density. A simple and robust solution-processable method is used for preparing the rGO/Fe_3O_4 NPs/PU flexible films. The rGO and PU can form a strong hydrogen bonding due to a lot of hydroxy groups, which results in a well-dispersed rGO in PU instead of agglomeration or restack. The permittivity value of the composites in a frequency range 0.1 GHz–18 GHz increases with annealing temperatures of GO increasing. For 5-wt% rGO/Fe_3O_4 NPs/PU, the maximum RL of over −35 dB appears at 4.5 GHz when the thickness of film increases to 5 mm. The main microwave absorption mechanism of rGO/Fe_3O_4 NPs/PU film is dielectric loss produced by relaxation process that includes interfacial polarization and electronic dipole polarization between rGO and PU, and good impedance match from the introduce of permeability of Fe_3O_4 NPs. Such an rGO/Fe_3O_4 NPs/PU flexible film can be used as effective microwave absorption material in the future flexible electronic devices.

References

[1] Kong L B, Li Z W, Liu L, Huang R, Abshinova M, Yang Z H, Tang C B, Tan P K, Deng C R and Matitsine S 2013 *Int. Mater. Rev.* **58** 203

[2] Chakraborty U, Chatterjee S, Chowdhury S K and Sarkar P P 2011 *Prog. Electromagn. Res. C* **18** 211

[3] Sun X, He J P, Li G X, Tang J, Wang T, Guo Y X and Xue H R 2013 *J. Mater. Chem. C* **1** 765

[4] Yang Z H, Li Z W, Yang Y H and Xu Z C 2014 *ACS Appl. Mater. Interfaces* **6** 21911

[5] Lv H L, Zhang H Q, Ji G G and Xu Z C 2016 *ACS Appl. Mater. Interfaces* **8** 6529

[6] Sebastian M T and Jantunen H 2008 *Int. Mater. Rev.* **53** 57

[7] Buerkle A, Sarabandi K and Mosallaei H 2005 *IEEE Trans. Anten. Propag.* **53** 1020

[8] Truong V T, Riddell S Z and Muscat R F 1998 *J. Mater. Sci.* **33** 4971

[9] Kim J, Khoh W H, Wee B H and Hong J D 2015 *RSC Adv.* **5** 9904

[10] Quan B, Shi W H, Ong S J H, Lu X C, Wang P L Y, Ji G B, Guo Y F, Zheng L R and Xu Z C 2019 *Adv. Funct. Mater.* **29** 1901236

[11] Li Q, Zhang Z, Qi L P, Liao Q L, Kang Z and Zhang Y 2019 *Adv. Sci.* **6** 8

[12] Zhang Y, Huang Y, Zhang T, Chang H, Xiao P, Chen H, Huang Z and Chen Y 2015 *Adv. Mater.* **27** 2049

[13] Chen D Z, Wang G S, He S, Liu J, Guo L and Cao M S 2013 *J. Mater. Chem. A* **1** 5996

[14] Wang T, Li Y, Wang, Liu L C, Geng S, Jia X, Yang F, Zhang L, Liu L, You B, Ren X and Yang H T 2015 *RSC Adv.* **5** 60114

[15] Zhang X J, Wang G S, Cao W Q, Wei Y Z, Cao M S and Guo L 2014 *RSC Adv.* **4** 19594

[16] Han M, Yin X, Kong L, Li M, Duan W, Zhang L and Cheng L 2014 *J. Mater. Chem. A* **2** 16403

[17] Huang J, Cheng S P, Chen Y X, Chen Z L, Luo H, Xia X H and Liu H B 2019 *J. Mater. Chem. A* **7** 16720

[18] Li C, Fu Y S, Wu Z, Xia J W and Wang X 2019 *Nanoscale* **11** 12997

[19] Li X, Lu S Y, Xiong Z G, Hu Y, Ma D, Lou W Q, Peng C, Shen M W and Shi X Y 2019 *Adv. Sci.* 08 August

[20] Zhang L, Wan X N, Duan W J, Qiu H, Hou J Q, Wang X R, Li H and Du X Y 2019 *J. Nanosci. Nanotechnol.* **19** 7664

[21] Mahmudzadeh M, Yari H, Ramezanzadeh B and Mahdavian M 2019 *J. Indus. Engi. Chem.* **78** 125

[22] Pena-Bahamonde J, San-Miguel V, Baselga J, Fernandez-Blazquez J P, Gedler G, Ozisik R and Cabanelas J C 2019 *Carbon* **151** 84

[23] Song N N, Yang H T, Ren X, Li Z A, Luo Y, Shen J, Dai W, Zhang X Q and Cheng Z H 2013 *Nanoscale* **5** 2804

[24] Hummers W S and Offeman R E 1958 *J. Am. Chem. Soc.* **80** 1339

[25] Liang Y, Wu D, Feng X and Müllen K 2009 *Adv. Mater.* **21** 1679

[26] Guo S J and Sun S H 2012 *J. Am. Chem. Soc.* **134** 2492

[27] Ma R S, Huan Q, Wu L M, Yan J H, Zhang Y Y, Bao L H, Liu Y Q, Du S X and Gao H J 2017 *Chin. Phys. B* **26** 066801

[28] Guo H, Wang X Y, Bao D L, Lu H L, Zhang Y Y, Li G, Wang Y L, Du S X and Gao H J 2019 *Chin. Phys. B* **28** 078103

[29] Tung V C, Allen M J, Yang Y and Kaner R B 2009 *Nat. Nano* **4** 25

[30] Song N N, Yang H T, Liu H L, Ren X, Ding H F, Zhang X Q and Cheng Z H 2013 *Sci. Rep.* **3** 3161

[31] Naito Y and Suetake K 1971 *IEEE Trans. Microwave Theory Tech.* **19** 65

[32] Davalos A L and Zanette A 1999 *Fundamentals* **of** Electromagnetism

[33] Kong L, Yin X, Zhang Y, Yuan X, Li Q, Ye F, Cheng L and Zhang L 2013 *J. Phys. Chem. C* **117** 19701

[34] Xue D S, Li F S, Fan X L and Wen F S 2008 *Chin. Phys. Lett.* **25** 4128

[35] Li X P, Deng Z M, Li Y, Zhang H B, Zhao S, Zhang Y, Wu X Y and Yu Z Z 2019 *Carbon* **147** 172

[36] Tang J M, Liang N, Wang L, Li J, Tian G, Zhang D, Feng S H and Yue H J 2019 *Carbon* **152** 575